J Materiomics 3 (2017) 273–279

Contents lists available at ScienceDirect

J Materiomics

journal homepage: www.journals.elsevier.com/journal-of-materiomics/

Grain boundary engineering with nano-scale InSb producing high performance $In_xCe_yCo_4Sb_{12+z}$ skutterudite thermoelectrics

Han Li [a], Xianli Su [a], Xinfeng Tang [a, *], Qingjie Zhang [a], Ctirad Uher [b], G. Jeffrey Snyder [c], Umut Aydemir [c, d, **]

[a] State Key Laboratory of Advanced Technology for Materials Synthesis and Processing, Wuhan University of Technology, Wuhan 430070, China
[b] Department of Physics, University of Michigan, Ann Arbor, MI 48109, USA
[c] Department of Materials Science and Engineering, Northwestern University, Evanston, IL 60208, USA
[d] Department of Chemistry, Koc University, Sariyer, Istanbul 34450, Turkey

ARTICLE INFO

Article history:
Received 7 July 2017
Received in revised form
26 July 2017
Accepted 27 July 2017
Available online 2 August 2017

Keywords:
Filled skutterudites
Nanocomposite
MS-SPS
Thermoelectric properties

ABSTRACT

Thermoelectric semiconductors based on $CoSb_3$ hold the best promise for recovering industrial or automotive waste heat because of their high efficiency and relatively abundant, lead-free constituent elements. However, higher efficiency is needed before thermoelectrics reach economic viability for widespread use. In this study, n-type $In_xCe_yCo_4Sb_{12+z}$ skutterudites with high thermoelectric performance are produced by combining several phonon scattering mechanisms in a panoscopic synthesis. Using melt spinning followed by spark plasma sintering (MS-SPS), bulk $In_xCe_yCo_4Sb_{12+z}$ alloys are formed with grain boundaries decorated with nano-phase of InSb. The skutterudite matrix has grains on a scale of 100–200 nm and the InSb nano-phase with a typical size of 5–15 nm is evenly dispersed at the grain boundaries of the skutterudite matrix. Coupled with the presence of defects on the Sb sublattice, this multi-scale nanometer structure is exceptionally effective in scattering phonons and, therefore, $In_xCe_yCo_4Sb_{12}$/InSb nano-composites have very low lattice thermal conductivity and high zT values reaching in excess of 1.5 at 800 K.

© 2017 The Chinese Ceramic Society. Production and hosting by Elsevier B.V. This is an open access article under the CC BY-NC-ND license (http://creativecommons.org/licenses/by-nc-nd/4.0/).

1. Introduction

In recent years much effort worldwide has focused on the development of novel thermoelectric materials that are able to directly convert heat into electricity [1]. Thermoelectric conversion can be applied effectively to the power generation by using sources such as industrial waste heat and solar energy and, in turn, make a positive impact on energy consumption and environmental concerns [2]. The promise is predicated on the availability of more efficient thermoelectric materials that would significantly exceed the efficiency of the current state-of-the-art thermoelectrics. The conversion efficiency of thermoelectric devices is determined chiefly by the dimensionless figure of merit, zT, defined as $zT = \alpha^2\sigma T/\kappa$, where α is the Seebeck coefficient, σ is the electrical conductivity, T is the absolute temperature, and κ is the total thermal conductivity comprising the electronic, lattice, and bipolar contributions ($\kappa = \kappa_E + \kappa_L + \kappa_B$).

Skutterudites, and specifically the filled forms of $CoSb_3$ compounds, are viewed as one of the best bulk candidate materials for efficient thermoelectric power generation because they approximate the paradigm of "Phonon-Glass-Electron-Crystal" [3], the concept that requires the material to have electronic properties of a very good crystalline material and heat transport characteristics of an amorphous (glassy) system [4]. $CoSb_3$ compounds possess some of the highest mobilities of all bulk semiconductors [5] and the desired low thermal conductivity can be achieved by filling the Sb-icosahedral voids in the $CoSb_3$ structure by foreign ions such as rare earths, alkaline earths, and other species (Fig. 1a) [6–11]. In particular, reports have been published describing In and/or Ce filled skutterudites display high figure of merits [12–17]. Further modifications of the electronic and phonon properties of $CoSb_3$ can be facilitated by substitutions on the Co and/or Sb sublattices [18,19]. The defect-controlled electronic structure calculations have

* Corresponding author.
** Corresponding author. Department of Materials Science and Engineering, Northwestern University, Evanston, IL 60208, USA.
E-mail addresses: tangxf@whut.edu.cn (X. Tang), umut.aydemir@northwestern.edu (U. Aydemir).
Peer review under responsibility of The Chinese Ceramic Society.

http://dx.doi.org/10.1016/j.jmat.2017.07.003
2352-8478/© 2017 The Chinese Ceramic Society. Production and hosting by Elsevier B.V. This is an open access article under the CC BY-NC-ND license (http://creativecommons.org/licenses/by-nc-nd/4.0/).

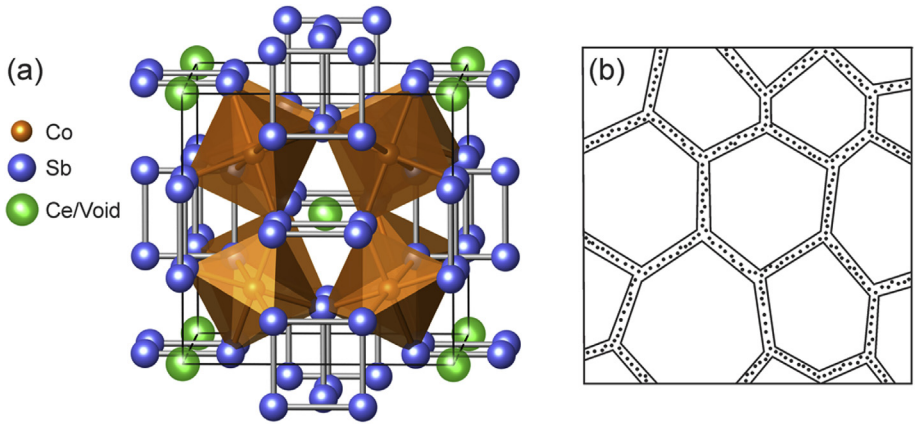


Fig. 1. (**a**) The crystal structure of $CoSb_3$ with $CoSb_6$ octahedra (shown in orange), Sb_4 rings, and void site that can be filled by other species like Ce or In (shown in transparent green). (**b**) A schematic microstructure with large grains of the skutterudite phase and InSb decorating the grain boundaries.

also provided further insights into tuning the carrier concentration in $CoSb_3$ [20,21].

Great improvements in the thermoelectric properties of a variety of materials have been accomplished by working with lower-dimensional structures [22,23] and by forming or embedding nano-composite features in the bulk matrix [24,25] (Fig. 1b). In general, bulk samples with nanostructural features are usually prepared in two distinct ways: reducing the grain size by physical processes such as ball milling [25] and metallurgical approaches to microstructure formation [26,27]. The formation of nanoparticles through near-equilibrium solid state transformation techniques are more likely to produce the clean, epitaxial (at a surface or interface) or endotaxial (within a grain) interfaces necessary for maintaining high charge carrier mobility across the interfaces as found with dislocations [28,29]. Metallurgical preparation techniques involving micron scale grain structure combined with nanometer sized precipitates and atomic scale point defects leads to a panoscopic approach in synthesizing these complex materials [30].

In previous studies on skutterudite-based nanocomposites, secondary nano-phases were (insulating) metal oxides such as Al_2O_3, Cu_2O, ZrO, Yb_2O_3, *etc*. [31–33] or more conducting Sb [34,35] or $FeSb_2$ [36]. Such nano-phases can markedly enhance scattering of phonons on grain boundaries that leads to an effective reduction in the lattice thermal conductivity [37]. Unfortunately, the presence of such nano-phases has usually led to a significant degradation of the electronic transport properties. Recently, it was shown that after applying additional sieving process before ball-milling, Al_2O_3 addition in $CoSb_3$ led to higher zT values [33]. In parallel, incorporating thin graphene-like carbon in grain interfaces can have only minor effect on electronic properties leading to a net benefit in zT [38]. A major challenge in composites is controlling the size and distribution of nano-phases due to agglomeration, uneven distribution, and uncontrolled growth during annealing and sintering stages of the process which leads to poor thermoelectric performance.

Herein, we show that nanoparticles of InSb can be made to form in the grain boundary interface, improving the scattering of heat carrying phonons without disrupting the electronic conductivity within the grains, ultimately producing higher efficiency material.

2. Experimental procedures

2.1. Materials preparation

Starting materials (In (99.999% shot), Ce (99.98% ingot), Co (99.99% shot), and Sb (99.9999% shot)) were weighed in stoichiometric amounts and loaded into a carbon-coated silica tube. The tube was sealed under a pressure of 10^{-5} mbar heated to 1373 K at 3 K/min, kept at this temperature for ~8–10 h, and then water-quenched. 10 g ingots were then inserted into a cylindrical quartz tube provided with a 0.3 mm diameter nozzle in our melt spinning (MS) apparatus where they were inductively melted under argon atmosphere (see Fig. S1). The melt was ejected under a pressure of 0.02 MPa of Ar onto the outer surface of a chilled spinning copper wheel where it was rapidly solidified in the form of thin ribbons of ~8–10 μm thickness and ~1.5–2 mm width. The linear speed of the outer diameter of the copper wheel was 30 m/s. In comparison to traditional method (TM), the yield for MS is relatively low, around 85%. The ribbons were collected, hand-ground, and subsequently loaded into a graphite die and sintered by the SPS method. Sintering was performed for 5 min under 40 MPa pressure at temperatures varying between 773 K and 873 K. The resulting nanostructured $In_xCe_yCo_4Sb_{12+z}$ bulk materials were 98% dense compared to the theoretical density. For comparison, we also prepared an $In_{0.15}Ce_{0.15}Co_4Sb_{12}$ sample by using the traditional melting-annealing-sintering route (see Fig. S2).

2.2. Structural characterization

For purposes of phase analysis, a small quantity of bulk samples of $In_xCe_yCo_4Sb_{12+z}$ after SPS were ground and examined by powder X-ray diffractometry (PANalytical: X′ Pert PRO) using an Inel diffractometer (Cu $K\alpha$ radiation) operating at 40 kV/40 mA. The microstructure and morphologies of the cross section of bulk materials sintered by SPS were investigated by the field emission scanning electron microscopy (FESEM, HITACHI S-4800). Finer microstructure and morphologies of bulk $In_xCe_yCo_4Sb_{12+z}$ ($x = 0.15$, 0.20; $y = 0.15$, 0.20; $z = 0$, 0.3) were examined using high-resolution transmission electron microscopy (HRTEM, JEM-2100F). Specimens used for the investigation were hand polished to about 50–60 μm with sand papers and subsequently with the diamond paste. Samples were then thinned down for electron transparency using a Gatan Model 600 CDIF precision ion-milling system at low angles (4–6°). High-resolution transmission electron microscopy images at several different locations were recorded at 200 kV. The elemental composition of ribbons and bulk samples were determined by energy dispersive X-ray (EDX) analysis. Electron probe microanalysis (EPMA) with a Cameca Camebax EPMA was employed to determine the actual chemical composition of the (sintered) skutterudite phase by using an accelerating

voltage of 15 keV and a current of 30 nA in a WDS mode and averaged over 10 randomly selected spots. The EPMA compositions (Table S1), agree with the nominal ones. Note that since the grain size of the InSb secondary phase is very small and homogenously distributed, this provides only an average composition of the measured area.

2.3. Thermoelectric characterization

The samples were cut into rectangular shapes of 3 mm × 3 mm × 8 mm for electrical property measurements (Fig. S3). The room temperature Hall measurements were carried out by use of a Qantum Design MPMS system combined with an AC Bridge used for data acquisition. Electrical conductivity (σ) and Seebeck coefficient (α) at high temperatures were measured synchronously by the standard four-probe method (ZEM-1, Ulvac Riko, Inc.) in an Ar atmosphere.

Thermal conductivity (κ) was calculated from the measured thermal diffusivity D, specific heat C_p, and density d using the relationship $\kappa = D \times C_p \times d$. Thermal diffusivity D was determined as a function of temperature using the flash diffusivity method (Netzsch LFA 457). The front face of a disk-shaped sample (~8 mm diameter and 1.5–2 mm thickness) was irradiated by a short laser burst, and the arrival of the thermal signal at the rear face was recorded and analyzed by an IR detector. C_p was measured using a power compensating differential scanning calorimeter (TA: DSC Q20) in N_2 atmosphere. The bulk density d was obtained by the Archimedes' method. All measurements were performed in the temperature range from 300 to 800 K. Sum of the lattice and bipolar thermal conductivities, ($\kappa_L+\kappa_B$), were obtained by subtracting the electronic contribution from the total thermal conductivity. Here, the electronic thermal conductivity is expressed by the Wiedemann Franz Law, $\kappa_E = LT\sigma$, where L is the Lorenz number calculated by $L = 1.5 + e^{-\frac{\alpha}{116}}$ where L is in 10^{-8} WΩK^{-2} and α in μV/K [39].

3. Results and discussion

3.1. Phase composition and microstructure

$CoSb_3$ is obtained in a peritectic reaction at 876 °C from $CoSb_2$ and the Sb-liquid phase [40]. The peritectic reaction is relatively slow and long annealing times are preferred to achieve the $CoSb_3$ phase as described in Fig. S2a, resulting in micrometer grain sizes. In contrast, the MS-SPS technique (see Fig. S2b) because of the ultra-high cooling rate (10^5 ~ 10^6 K/sec) of the melt produces a fine nanometer-scale grain size and a homogeneous distribution of the elements. Besides the main skutterudite phase, a small amount of cubic InSb phase is observed (nearly invisible because of small grain size) in the XRD of the $In_xCe_yCo_4Sb_{12+z}$ samples (see Fig. 2).

Field Emission Scanning Electron Microscopy (FESEM) photographs of the free surface fracture of the $In_{0.15}Ce_{0.15}Co_4Sb_{12}$ bulk sample prepared by TM (Fig. 3a and (b)) show a multiscale microstructure: micron sized grains of skutterudite with nanoparticles of InSb decorating the grain boundaries. A non-uniform size distribution (~1–5 μm) of these coarse grains is seen in Fig. 3a, which is a typical microstructure of filled skutterudites prepared by the traditional synthesis method. However it is not typical to observe nano-particles with ~20–100 nm size on the grain boundaries as in Fig. 3b. For the TM sample, FESEM analysis shows that nano-phases are not evenly dispersed and many grains and boundaries are clean and free of the presence of these nano-phases (see Fig. S4).

In contrast, when the MS-SPS technique is used to prepare the $In_{0.15}Ce_{0.15}Co_4Sb_{12}$ bulk sample (Fig. 3c), the grain size of the skutterudite matrix is drastically reduced down to ~150–300 nm with InSb decorated grain boundaries throughout. Besides crystallization of the matrix skutterudite phase, the nano-particles become finer (~10–15 nm, Fig. 3d). More important, the distribution of nano-scale-secondary-phase is more uniform in the nanostructured skutterudite matrix and these nano-particles can be observed almost everywhere.

As shown in high-resolution transmission electron microscopy (HRTEM) image (Fig. 4a), the grain size of the MS-SPS sample is around 150–200 nm and all grains are tightly spaced. In addition, high-resolution images (Fig. 4b and c) demonstrate that even finer nano-particles (5–15 nm) are present at the grain boundaries, in agreement with the FESEM results. Fig. 4b displays a 15 nm InSb particle (marked as domain IV) in the grain-boundary between three large grains (I, II and III) of filled skutterudite. The EDX confirms domains I, II and III possess similar elemental composition of Ce, Co and Sb (Co/Sb ≈ 1/3). The interplanar distance measured in domain I of 0.285 nm corresponds to the (013) interplanar distance of 0.286 nm in $CoSb_3$. Domain IV, rich in In (by EDX) and having interplanar distance of 0.323 nm, is identified as the (200) planes of InSb (0.324 nm). Similarly, the interplanar spacing seen in the 5–10 nm grains in Fig. 3c being 0.276–0.277 nm can be identified as InSb (101) (~0.277 nm).

In this study, the composite containing grain boundaries decorated with InSb nanoparticles must be formed by rapid nucleation of InSb at the grain boundaries. InSb has some solubility in $CoSb_3$ in the solid state with In able to substitute for Sb as well as fill the void site forming charge-compensated compound defects [17]. The solubility of In is expected to be highly temperature dependent, as observed for other filling atoms, *e.g.,* Yb [10] and Ce [16], forming a skutterudite phase super-saturated with the filler atom during the rapid solidification process. As the solid cools, InSb should precipitate but is kinetically stabilized due to lack of nucleation sites. The grain boundaries provide epitaxial nucleation sites and attract InSb from nearby areas. The high cooling rate produces a large degree of supersaturation and high nucleation density in the grain boundaries [27]. The small grain size ensures the InSb precipitates grow to a limited size by removing InSb from the grain interior by diffusion. This diffusion limited process ultimately produces many small InSb coherent nanoparticles that are effective phonon scatterers but are minimally disruptive to electrons.

3.2. Thermoelectric transport properties

It is clear that electrical conductivity and carrier concentration increase with the increasing In and Ce doping level for the MS-SPS samples (Fig. 5a and b, see Table S1), while excess Sb has been used to enhance the electrical conductivity [41] and compensate for the loss of Sb during the processing. When $x = y = 0.15$ and $z = 0$, the electrical conductivity of the TM sample is higher than that of the MS-SPS sample due to the larger grain size.

Seebeck values are found to be very close to those of single filled Ce doped compounds (see Fig. S5) [16]. Solely In doped compounds have lower conductivity along with higher Seebeck coefficients, due to charge-compensated point defects [17]. As no Ce containing secondary phase is found by XRD and microstructure analysis, Ce may act as the main filler in this crystal structure. Based on the recent study by Tang et al. [16], the filling fraction limit of Ce in the skutterudite phase may reach as high as $y = 0.2$, which exceeds the amount of Ce used in the current study. Recently, the formation energies of the skutterudite phase with different filler atoms (electropositive or electronegative guests) were reported [6]. It was shown in this study that compared to the group III elements as filler atom (*e.g.*, Ga), compositions with alkali metals, alkaline earth metals, and rare earths having much lower electronegativity (higher electropositivity) are thermodynamically more stable.

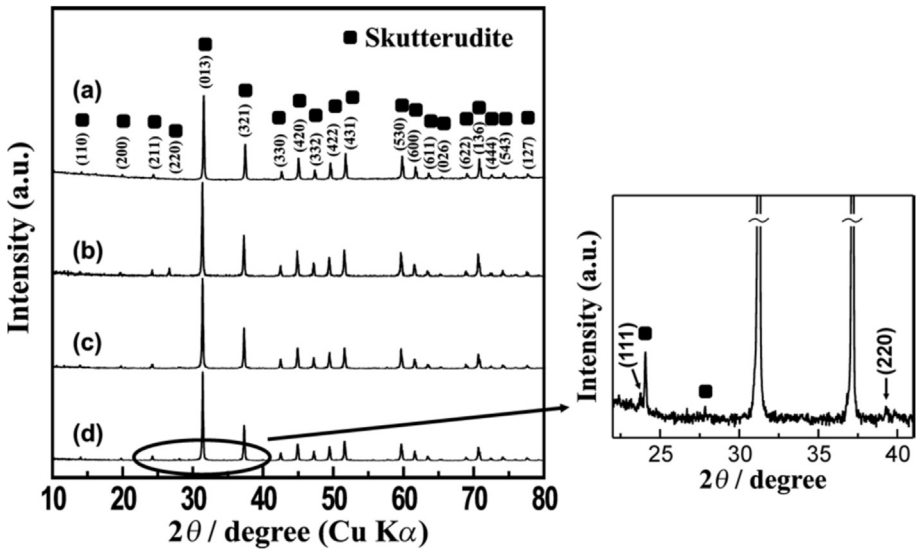


Fig. 2. XRD patterns of bulk $In_xCe_yCo_4Sb_{12+z}$ prepared by MS-SPS: (**a**) $x = 0.15$, $y = 0.15$; (**b**) $x = 0.2$, $y = 0.15$; (**c**) $x = 0.2$, $y = 0.15$, $z = 0.3$; (**d**) $x = 0.2$, $y = 0.2$. The arrows in the right figure show (cubic) InSb XRD peaks with very low intensities.

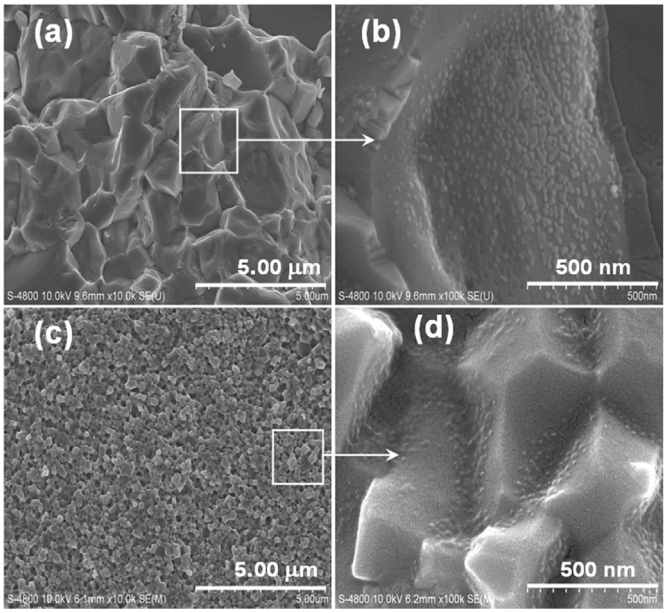


Fig. 3. FESEM photographs of the free surface fracture of $In_{0.15}Ce_{0.15}Co_4Sb_{12}$ bulk sample prepared by different methods. (**a**) The sample prepared by TM and (**b**) magnified image of (a). (**c**) The sample prepared by MS-SPS and (**d**) magnified images of (c).

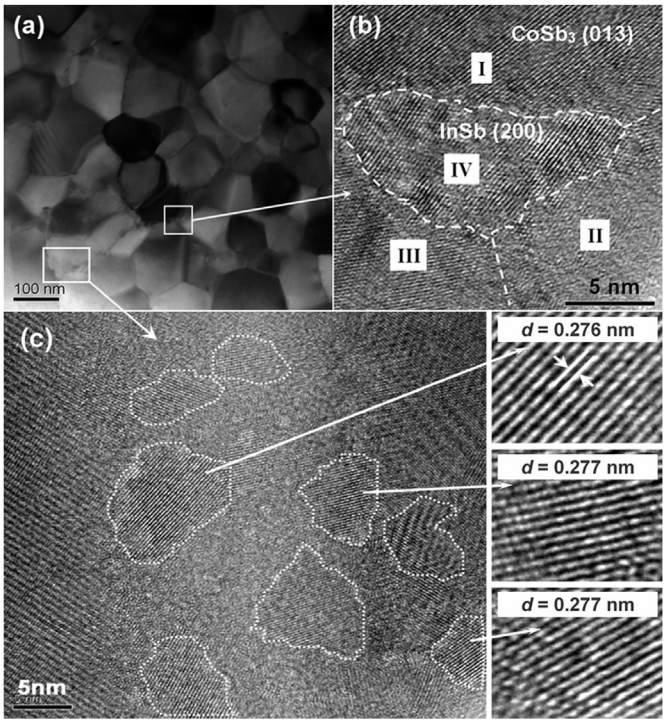


Fig. 4. (**a**) HRTEM images of MS-SPS-prepared $In_{0.15}Ce_{0.15}Co_4Sb_{12}$ bulk sample, (**b**) high resolution image of grain boundary phase, and (**c**) high resolution image of a region with several InSb grain boundary nanoparticles.

When x and y are fixed, samples with $z = 0.3$ show higher electrical conductivity than the samples with $z = 0$. This indicates that a small excess of Sb indeed improves the electrical conductivity of n-type skutterudites. It is noteworthy to point out that, although MS-SPS samples possess a nano-crystalline structure and a finer nano-InSb phase evenly dispersed on their grain boundaries, they still show very high value of electrical conductivity compared with the case of insulating nano-oxide composite skutterudites [31,36]. The Seebeck coefficient of most $In_xCe_yCo_4Sb_{12+z}$/InSb samples has a magnitude exceeding 200 μVK^{-1} at 800 K. Previously it was reported that inclusion of nanoparticles or formation of nano-grains may lead to quantum confinement or electron filtering effects that benefit the Seebeck coefficient [22,42]. To check for such effects, we compare the data using a plot of Seebeck coefficient vs. Hall carrier concentration (known as Pisarenko plot) at room temperature which can also be used to extract an average Seebeck effective mass m^* [43]. The measured Seebeck values at these carrier concentrations (effective mass m^*) are found to be very similar to the ones in typical n-type $CoSb_3$ [44]. From this we conclude that nano-grains (~100–200 nm) of the skutterudite phase and nano-precipitates (5–10 nm) of InSb secondary phase don't lead to pronounced enhancement of Seebeck coefficient (at room temperature) as discussed for other low dimensional or nano-

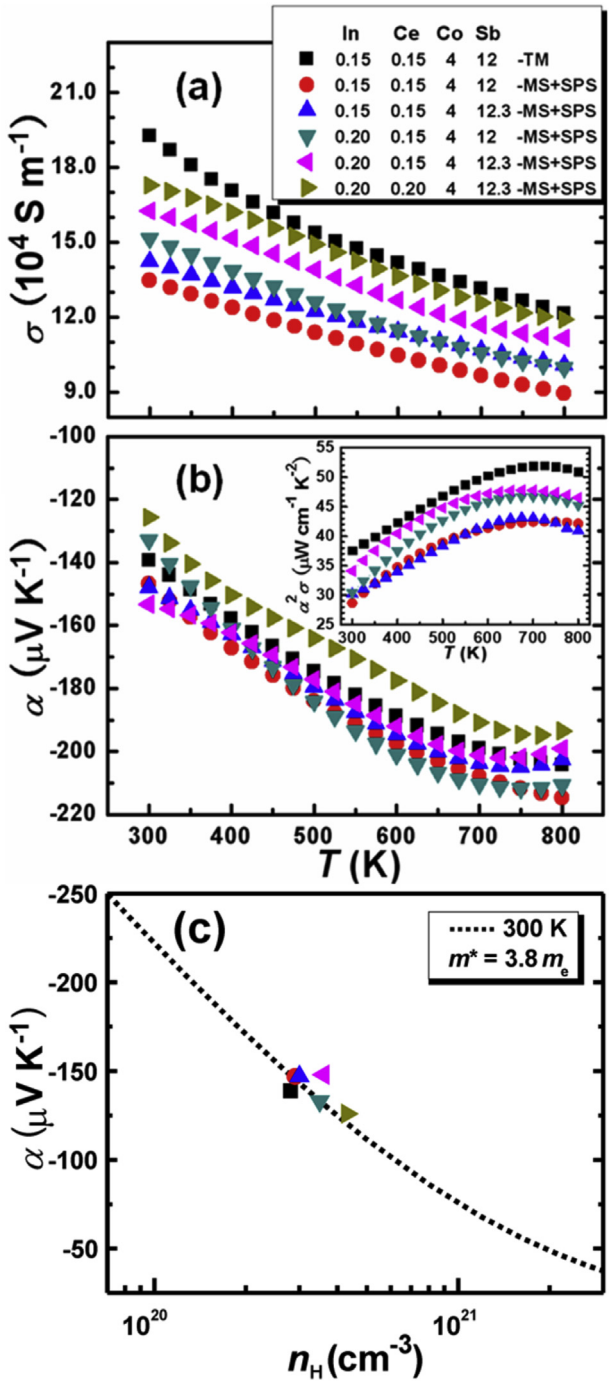


Fig. 5. Temperature dependence of (**a**) electrical conductivity and (**b**) Seebeck coefficient. The inset of (b) shows the power factor for $In_xCe_yCo_4Sb_{12+z}$/InSb nanocomposites. (**c**) Pisarenko plot of the samples used to extract an average Seebeck effective mass m^* at room temperature.

sized systems. As shown in the inset of Fig. 5b, all $In_xCe_yCo_4Sb_{12+z}$/InSb samples show very high power factors. The power factor of the TM sample is higher than the MS-SPS processed samples because degraded electrical conductivity of the MS-SPS samples is not fully compensated by their enhanced Seebeck coefficients. We also note that, as far as the power factor is concerned, for a fixed x and y, the excess of Sb has a negligible effect.

The most important benefit of nanostructuring comes in the form of a dramatically reduced thermal conductivity. As shown in Fig. 6a, the thermal conductivity of the MS-SPS samples is much lower than that of the TM sample. For the same composition, κ of the MS-SPS-prepared $In_{0.15}Ce_{0.15}Co_4Sb_{12}$ at 300 K is 2.28 W $m^{-1}K^{-1}$ while κ of the TM-prepared $In_{0.15}Ce_{0.15}Co_4Sb_{12}$ at the same temperature is 3.52 W $m^{-1}K^{-1}$, a reduction of some 35%. At 800 K the reduction amounts to 25%. The κ_L of the MS-SPS-prepared $In_{0.15}Ce_{0.15}Co_4Sb_{12}$/InSb sample is markedly reduced compared to that of the TM-prepared $In_{0.15}Ce_{0.15}Co_4Sb_{12}$/InSb (Fig. 6b). The reduction in the lattice thermal conductivity has two origins: the nanostructured skutterudite matrix; and even finer and evenly distributed nano-InSb phase at the grain boundaries. It is also important to note that when x and y are fixed, the lattice thermal conductivity increases with z. This means that phonon transport is more inhibited in samples that are not compensated for the loss of Sb. We surmise that a distinctly lower lattice thermal conductivity of samples in the $In_xCe_yCo_4Sb_{12}$/InSb series in comparison to those of $In_xCe_yCo_4Sb_{12+z}$/InSb (Fig. 6b) has a more subtle origin. From the structural studies we know that the presence of In in the skutterudite matrix mostly leads to the formation of InSb nano-phase and, as shown in Fig. 2, no other phase is detected except for the skutterudite matrix. Thus, $In_xCe_yCo_4Sb_{12}$/InSb compounds (the compounds with $z = 0$) may have a slight deficiency of Sb in the skutterudite matrix and therefore vacancies or In substitution on the Sb sublattice. Such point defects may scatter effectively short wavelength phonons and, although they do not dominate heat transport, the thermal conductivity can be further suppressed by including this scattering. In fact, a multiple nano-scale composite structure such as our MS-SPS-prepared $In_xCe_yCo_4Sb_{12}$/InSb (nanostructured skutterudite matrix on the scale of ~200 nm; nano-phase of InSb with a typical scale of 5–15 nm; and point defects on the Sb sublattice) should strongly scatter a broad spectrum of phonons and thus reduce the thermal conductivity very effectively. The values of the lattice thermal conductivity shown in Fig. 6b attest to it.

The dimensionless thermoelectric figure of merit zT is displayed in Fig. 6c. All $In_xCe_yCo_4Sb_{12}$/InSb samples show high zT values which are largely due to a strongly suppressed lattice thermal conductivity while maintaining very good electrical transport properties. The maximum value of the dimensional figure of merit of ~1.5 is achieved on the MS-SPS-processed $In_{0.2}Ce_{0.15}Co_4Sb_{12}$/InSb sample at 800 K. Compared with the traditional method, the application of MS-SPS technique may further enhance the zT by 15%. We also estimated zT as a function of Hall carrier concentration at 300 K based on the quality factor model by assuming a constant κ_L (Fig. 6d). Based on Fig. 6d, the optimum carrier concentration of the skutterudite compounds is found to be ~1.25×10^{20} e^-/cm^3. Current samples have slightly higher carrier concentrations than the optimal one. Therefore, further enhancement of the thermoelectric efficiencies is possible by tuning the charge carrier concentration in this system.

4. Conclusions

In this study, we successfully prepared n-type skutterudite with small grain size and point defects that have nanoparticles decorating the grain boundaries for added phonon scattering. We used an MS-SPS synthetic route for the preparation of n-type $In_xCe_yCo_4Sb_{12+z}$/InSb and applied double filling, In and Ce, to control the doping and the microstructure independently. Ce is an excellent dopant that goes on the filler site, in addition, Indium has limited solubility and easily forms a secondary phase (especially when In is co-doped with Ce) consisting of a uniformly distributed nano-grains of InSb. The resulting material has dramatically reduced thermal conductivity that leads to a high performance thermoelectric material with zT_{max} in excess of 1.5 at 800 K.

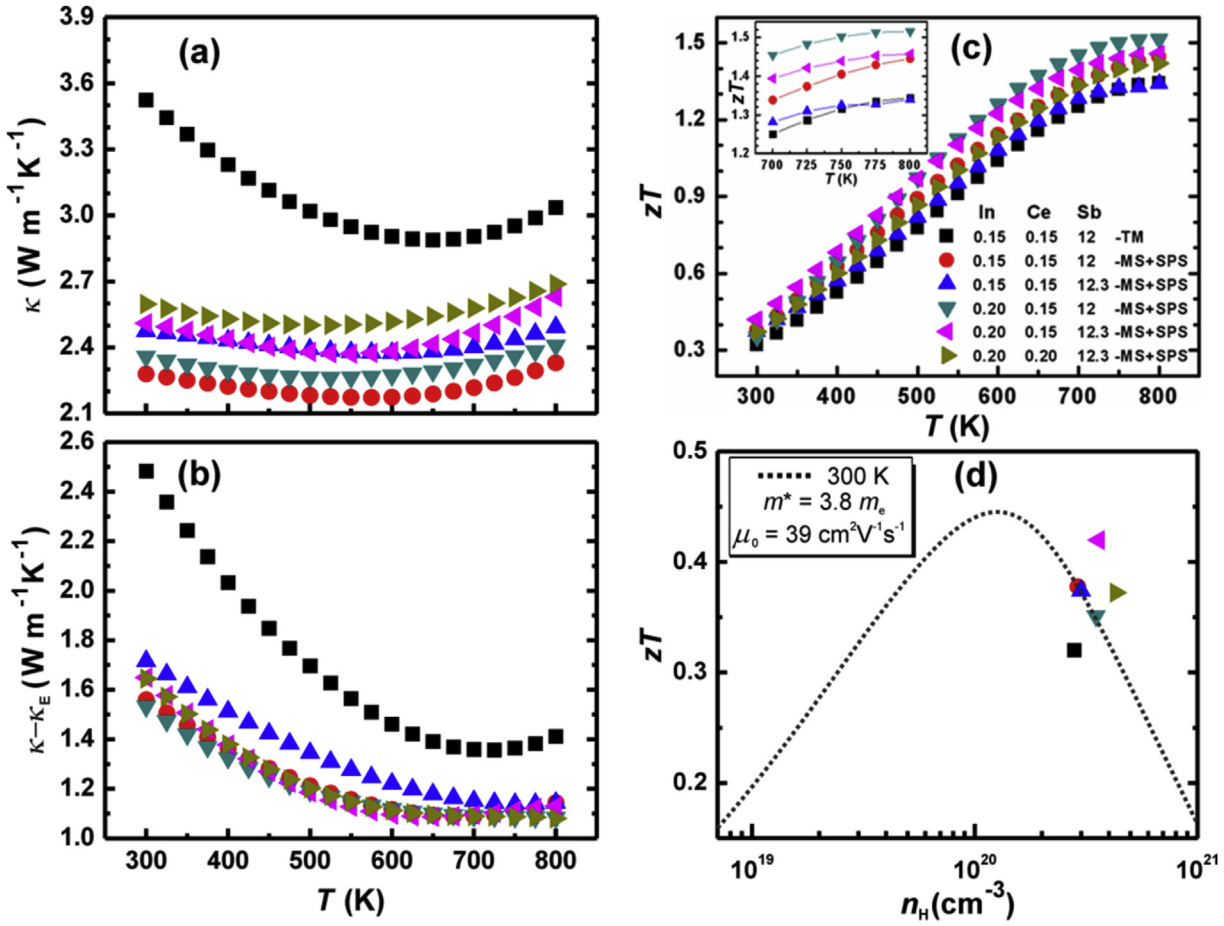


Fig. 6. Temperature dependences of (**a**) total thermal conductivity and (**b**) sum of the lattice and bipolar thermal conductivity of $In_xCe_yCo_4Sb_{12+z}$/InSb nano-composites (The contribution of κ_B is considered to be negligible below 650 K). (**c**) Temperature dependence of zT for $In_xCe_yCo_4Sb_{12+z}$/InSb nano-composites. (**d**) Experimental zT values at 300 K showing that all the samples are over-doped compared to the optimal carrier concentration based on the quality factor model.

Engineering grain boundaries and not just making them opens new possibilities for improving functional materials.

Acknowledgments

H.L., X.T., and Q.Z. acknowledge financial supports of the National Basic Research Program of China (Grant No. 2013CB632502), Natural Science Foundation of China (Grant Nos. 51402222, 51172174, and 51002112), and the 111 Project of China (Grant No. B07040). U.A. and G.J.S. acknowledge funding from the Solid-State Solar-Thermal Energy Conversion Center (S3TEC), an Energy Frontier Research Center, funded by the U.S. Department of Energy, Office of Science, Basic Energy Sciences (DE-SC0001299).

Appendix A. Supplementary data

Supplementary data related to this article can be found at http://dx.doi.org/10.1016/j.jmat.2017.07.003.

References

[1] Snyder GJ, Toberer ES. Complex thermoelectric materials. Nat Mater 2008;7:105–14.
[2] Shi X, Chen L, Uher C. Recent advances in high-performance bulk thermoelectric materials. Int Mater Rev 2016;61:379–415.
[3] Rull-Bravo M, Moure A, Fernandez JF, Martin-Gonzalez M. Skutterudites as thermoelectric materials: revisited. Rsc Adv 2015;5:41653–67.
[4] Nolas GS, Morelli DT, Tritt TM. SKUTTERUDITES: a phonon-glass-electron crystal approach to advanced thermoelectric energy conversion applications. Annu Rev Mater Sci 1999;29:89–116.
[5] Arushanov E, Fess K, Kaefer W, Kloc C, Bucher E. Transport properties of lightly doped CoSb3 single crystals. Phys Rev B 1997;56:1911–7.
[6] Duan B, Yang J, Salvador JR, He Y, Zhao B, Wang SY, et al. Electronegative guests in CoSb3. Energ Environ Sci 2016;9:2090–8.
[7] Graff JW, Zeng X, Dehkordi AM, He J, Tritt TM. Exceeding the filling fraction limit in CoSb3 skutterudite: multi-role chemistry of praseodymium leading to promising thermoelectric performance. J Mater Chem A 2014;2:8933–40.
[8] Li YL, Qiu PF, Duan HZ, Chen JK, Snyder GJ, Shi X, et al. Enhanced thermoelectric performance in rare-earth filled-skutterudites. J Mater Chem C 2016;4:4374–9.
[9] Qiu YT, Xi LL, Shi X, Qiu PF, Zhang WQ, Chen LD, et al. Charge-compensated compound defects in Ga-containing thermoelectric skutterudites. Adv Funct Mater 2013;23:3194–203.
[10] Tang Y, Chen S-w, Snyder GJ. Temperature dependent solubility of Yb in Yb–CoSb3 skutterudite and its effect on preparation, optimization and lifetime of thermoelectrics. J Materiomics 2015;1:75–84.
[11] Xi LL, Qiu YT, Zheng S, Shi X, Yang J, Chen LD, et al. Complex doping of group 13 elements In and Ga in caged skutterudite CoSb3. Acta Mater 2015;85:112–21.
[12] Graff J, He J, Tritt T. Qualifying the role of indium in the multiple-filled Ce0.1InxYb0.2Co4Sb12 skutterudite. Inorganics 2014;2:168.
[13] Li H, Tang X, Zhang Q, Uher C. High performance InxCeyCo4Sb12 thermoelectric materials with in situ forming nanostructured InSb phase. Appl Phys Lett 2009;94:102114.
[14] Rogl G, Grytsiv A, Yubuta K, Puchegger S, Bauer E, Raju C, et al. In-doped multifilled n-type skutterudites with ZT=1.8. Acta Mater 2015;95:201–11.
[15] Sesselmann A, Klobes B, Dasgupta T, Gourdon O, Hermann R, Mueller E. Neutron diffraction and thermoelectric properties of indium filled InxCo4Sb12 (x = 0.05, 0.2) and indium cerium filled Ce0.05In0.1Co4Sb12 skutterudites. Phys Status Solidi A 2016;213:766–73.
[16] Tang Y, Hanus R, Chen S-w, Snyder GJ. Solubility design leading to high figure of merit in low-cost Ce-CoSb3 skutterudites. Nat Commun 2015;6:7584.
[17] Tang Y, Qiu Y, Xi L, Shi X, Zhang W, Chen L, et al. Phase diagram of In-Co-Sb

system and thermoelectric properties of In-containing skutterudites. Energ Environ Sci 2014;7:812–9.
[18] Jung J-Y, Ur S-C, Kim I-H. Thermoelectric properties of InzCo4Sb12−yTey skutterudites. Mater Chem Phys 2008;108:431–4.
[19] Zevalkink A, Star K, Aydemir U, Jeffrey Snyder G, Fleurial J-P, Bux S, et al. Electronic structure and thermoelectric properties of pnictogen-substituted ASn1.5Te1.5 (A = Co, Rh, Ir) skutterudites. J Appl Phys 2015:118. 035107.
[20] Li GD, Aydemir U, Wood M, Goddard WA, Zhai PC, Zhang QJ, et al. Defect-controlled electronic structure and phase stability in thermoelectric skutterudite CoSb3. Chem Mater 2017;29:3999–4007.
[21] Li G, Bajaj S, Aydemir U, Hao S, Xiao H, Goddard III WA, et al. P-type Co interstitial defects in thermoelectric skutterudite CoSb3 due to the breakage of Sb4-rings. Chem Mater 2016;28:2172–9.
[22] Dresselhaus MS, Chen G, Tang MY, Yang RG, Lee H, Wang DZ, et al. New directions for low-dimensional thermoelectric materials. Adv Mater 2007;19: 1043–53.
[23] Heremans JP. Low-dimensional thermoelectricity. Acta Phys Pol A 2005;108: 609–34.
[24] Hsu KF, Loo S, Guo F, Chen W, Dyck JS, Uher C, et al. Cubic AgPbmSbTe2+m: bulk thermoelectric materials with high figure of merit. Science 2004;303: 818–21.
[25] Liu W, Yan X, Chen G, Ren Z. Recent advances in thermoelectric nanocomposites. Nano Energy 2012;1:42–56.
[26] Biswas K, He JQ, Zhang QC, Wang GY, Uher C, Dravid VP, et al. Strained endotaxial nanostructures with high thermoelectric figure of merit. Nat Chem 2011;3:160–6.
[27] Heinz NA, Ikeda T, Pei YZ, Snyder GJ. Applying quantitative microstructure control in advanced functional composites. Adv Funct Mater 2014;24: 2135–53.
[28] Chen Z, Ge B, Li W, Lin S, Shen J, Chang Y, et al. Vacancy-induced dislocations within grains for high-performance PbSe thermoelectrics. Nat Commun 2017;8:13828.
[29] Kim SI, Lee KH, Mun HA, Kim HS, Hwang SW, Roh JW, et al. Dense dislocation arrays embedded in grain boundaries for high-performance bulk thermoelectrics. Science 2015;348:109–14.
[30] Zhao LD, Dravid VP, Kanatzidis MG. The panoscopic approach to high performance thermoelectrics. Energ Environ Sci 2014;7:251–68.
[31] Zhao XY, Shi X, Chen LD, Zhang WQ, Bai SQ, Pei YZ, et al. Synthesis of YbyCo4Sb12/Yb2O3 composites and their thermoelectric properties. Appl Phys Lett 2006:89. 092121.
[32] Zeming H, Christian S, Dieter P, Gabriele K, Eckhard M, Shanghua L, et al. Nano ZrO 2/CoSb 3 composites with improved thermoelectric figure of merit. Nanotechnology 2007;18. 235602.
[33] Rogl G, Grytsiv A, Failamani F, Hochenhofer M, Bauer E, Rogl P. Attempts to further enhance ZT in skutterudites via nano-composites. J Alloy Compd 2017;695:682–96.
[34] Li H, Tang X, Su X, Zhang Q. Preparation and thermoelectric properties of high-performance Sb additional Yb0.2Co4Sb12+y bulk materials with nanostructure. Appl Phys Lett 2008;92. 202114.
[35] Li H, Tang X, Zhang Q, Uher C. Rapid preparation method of bulk nanostructured Yb0.3Co4Sb12+y compounds and their improved thermoelectric performance. Appl Phys Lett 2008;93. 252109.
[36] Katsuyama S, Kanayama Y, Ito M, Majima K, Nagai H. Thermoelectric properties of CoSb3 with dispersed FeSb2 particles. J Appl Phys 2000;88:3484–9.
[37] Eilertsen J, Surace Y, Balog S, Sagarna L, Rogl G, Horky J, et al. From occupied voids to nanoprecipitates: synthesis of skutterudite nanocomposites in situ. Z Anorg Allg Chem 2015;641:1495–502.
[38] Zong PA, Hanus R, Dylla M, Tang YS, Liao JC, Zhang QH, et al. Skutterudite with graphene-modified grain-boundary complexion enhances zT enabling high-efficiency thermoelectric device. Energ Environ Sci 2017;10:183–91.
[39] Kim H-S, Gibbs ZM, Tang Y, Wang H, Snyder GJ. Characterization of Lorenz number with Seebeck coefficient measurement. APL Mater 2015:3. 041506.
[40] Massalski TB. ASM International. Binary alloy phase diagrams. second ed. Materials Park, Ohio: ASM International; 1990.
[41] Yu J, Zhao WY, Wei P, Tang DG, Zhang QJ. Effects of excess Sb on thermoelectric properties of barium and indium double-filled iron-based p-type skutterudite materials. J Electron Mater 2012;41:1414–20.
[42] Zide JMO, Vashaee D, Bian ZX, Zeng G, Bowers JE, Shakouri A, et al. Demonstration of electron filtering to increase the Seebeck coefficient in ErAs: InGaAs/InGaAlAs superlattices. Phys Rev B 2006;74:205335.
[43] May AF, Snyder GJ. Introduction to modelling thermoelectric transport at High Temperatures. In: Rowe DM, editor. Materials, preparation and characterization in thermoelectrics. Boca Raton, FL: Taylor & Francis Group; 2012. 11–1, -8.
[44] Tang Y, Gibbs ZM, Agapito LA, Li G, Kim H-S, Nardelli MB, et al. Convergence of multi-valley bands as the electronic origin of high thermoelectric performance in CoSb3 skutterudites. Nat Mater 2015;14:1223–8.



Prof. Han Li received his Ph.D. in Materials Science and Engineering from Wuhan University of Technology of China in 2009, upon which he started working as an Associate Professor. From 2013 to 2016, he worked as a visiting scholar in the department of Engineering and Applied Science at the California Institute of Technology, USA. His research focuses on the novel thermoelectric materials and their applications. Prof. Li has been selected as the recipient of the 2009 International Thermoelectric Society Goldsmid Award.



Prof. Xinfeng Tang received his Ph.D. from Tohoku University of Japan in 2000. He joined in Wuhan University of Technology as a full professor in April, 2001. Now he is the Deputy Executive Director of the State Key Laboratory of Advanced Technology for Materials Synthesis and Processing, Director of the Advanced Materials Research Institute. He has been a Chair Professor of materials science since 2011, and a Fellow of the American Physical Society and a board member of International Thermoelectric Society.



Dr. Umut Aydemir is a research associate working with Prof. G. Jeffrey Snyder in the Department of Materials Science and Engineering at Northwestern University. He received his B.Sc. in Chemistry and Physics and M.Sc. in Materials Science and Engineering at Koç University in Istanbul, Turkey. He conducted his graduate work at the Max Planck Institute for Chemical Physics of Solids in Dresden, Germany studying synthesis and characterization of intermetallic clathrates with Prof. Yuri Grin. His research interests include synthesis and characterization of thermoelectric materials and investigation of electrical and thermal transport properties of solids. His work has resulted in the publication of over 50 research papers.